Remote Sensing of Environment 113 (2009) 2142–2151

Contents lists available at ScienceDirect

Remote Sensing of Environment

journal homepage: www.elsevier.com/locate/rse

ASTER- and field-based observations at Bezymianny Volcano: Focus on the 11 May 2007 pyroclastic flow deposit

Adam J. Carter *, Michael S. Ramsey

Department of Geology and Planetary Science, University of Pittsburgh, Pittsburgh, PA 15260, USA

ARTICLE INFO

Article history:
Received 21 November 2008
Received in revised form 29 May 2009
Accepted 30 May 2009

Keywords:
Volcanology
Remote sensing
Bezymianny
Pyroclastic flow deposits
Thermal infrared

ABSTRACT

Bezymianny (Kamchatka Peninsula, Russia) is an active stratovolcano, characterized by a summit lava dome and overlapping pyroclastic flow (PF) deposits to the southeast. Three explosive eruptions (24 December 2006, 11 May 2007, and 14 October 2007) generated PFs that were dominated by juvenile material and were emplaced primarily due to column collapse. Following this, a gravitational lava flow front collapse event generated block and ash flow on 5 November 2007. Moderate spatial resolution data from the Advanced Spaceborne Thermal Emission and Reflection Radiometer (ASTER) instrument were collected between October 2006 and December 2007 to assist in post-eruption monitoring and interpretation of the volcanological processes that produced the PF deposits. Using multitemporal ASTER thermal infrared (TIR) data, three periods of increased activity were observed that coincided with each eruption and subsequent activity. During a field campaign in August 2007, the May 2007 PF deposit was investigated in detail. Eight ASTER TIR pixels (90 m spatial resolution) were selected from the 30 June 2007 ASTER TIR image, seven of which were accessible in the field. Forward-Looking Infrared (FLIR) image and thermocouple data over these areas were collected to observe thermal heterogeneities with distance along the PF deposit. Although synchronous ASTER data were not possible at the time of fieldwork due to cloud cover, a field survey of blocks versus ash in each pixel was carried out to investigate thermal and textural variation with distance from the vent and to provide preliminary field results. Based on the field-derived temperature data and surface block percentages, the May 2007 PF deposit was more block-rich in the medial portion of the flow surface, but more ash-dominated at the PF terminus region, which promoted more rapid cooling. We present multitemporal ASTER data spanning a 14 month period and highlight ground-based observations acquired within the same period of eruptive and dome-growth activity. These data collectively provide thermal radiative and emissivity information on an actively changing explosive volcanic system and specifically documents changes over recently-emplaced and cooling PF deposits.

1. Introduction

1.1. North Pacific volcanism and ongoing activity at Bezymianny Volcano

North Pacific volcanism has been monitored in detail since the 1990's with the formation of Alaska Volcano Observatory (AVO) and the Kamchatka Volcano Eruption Response Team (KVERT). ASTER data have been collected since 2000 over the Kamchatka Peninsula of Russia and Bezymianny in particular was selected as a target of interest due to its moderate/high activity levels and overlapping pyroclastic flow sheet (Ramsey & Dehn, 2004; Carter et al., 2008).

Bezymianny (55.98° N, 160.59° E, ~2900 m altitude) is an andesite volcano located 350 km north of Petropavlovsk–Kamchatsky, Russia (Bogoyavlenskaya et al., 1991; Fig. 1). The volcano was inactive for approximately one thousand years before the cataclysmic eruption of 30 March 1956 (Gorshkov, 1959; Belousov, 1996; Belousov et al., 2007). This generated a 1.3 km (north–south) by 2.8 km (east–west) horseshoe-shaped crater opening to the southeast. Subsequently, a long-term phase of lava dome growth began in the crater, which was mostly endogenous prior to 1969 (Bogoyavlenskaya and Kirsanov, 1981). Exogenous dome activity became more common after 1977 (Alidibirov et al., 1990; Bogoyavlenskaya & Kirsanov, 1981). During the last 30 years, Bezymianny has been regularly active, erupting one or two times per year on average (Belousov et al., 2002; Ramsey and Dehn, 2004; Carter, Ramsey, Belousov, 2007; Carter et al., 2009). However, this activity has been punctuated by much larger events such as the sub-Plinian eruptions of 1985 and 1997 (Alidibirov et al., 1990; Belousov et al., 2002) and the more recent 9 May 2006 eruption (KVERT, 2007). This history makes Bezymianny an important volcano to monitor because it is not only a threat to the sparse local population but is also capable of producing ash-rich plumes that can drift into North Pacific air traffic routes (Miller & Casadevall, 2000; Papp et al., 2005).

Volcanic activity at Bezymianny is dominantly explosive and can generate ash plumes that create ash fall, pyroclastic flow, and

* Corresponding author.
E-mail address: carteradam09@gmail.com (A.J. Carter).

0034-4257/$ – see front matter © 2009 Elsevier Inc. All rights reserved.
doi:10.1016/j.rse.2009.05.020

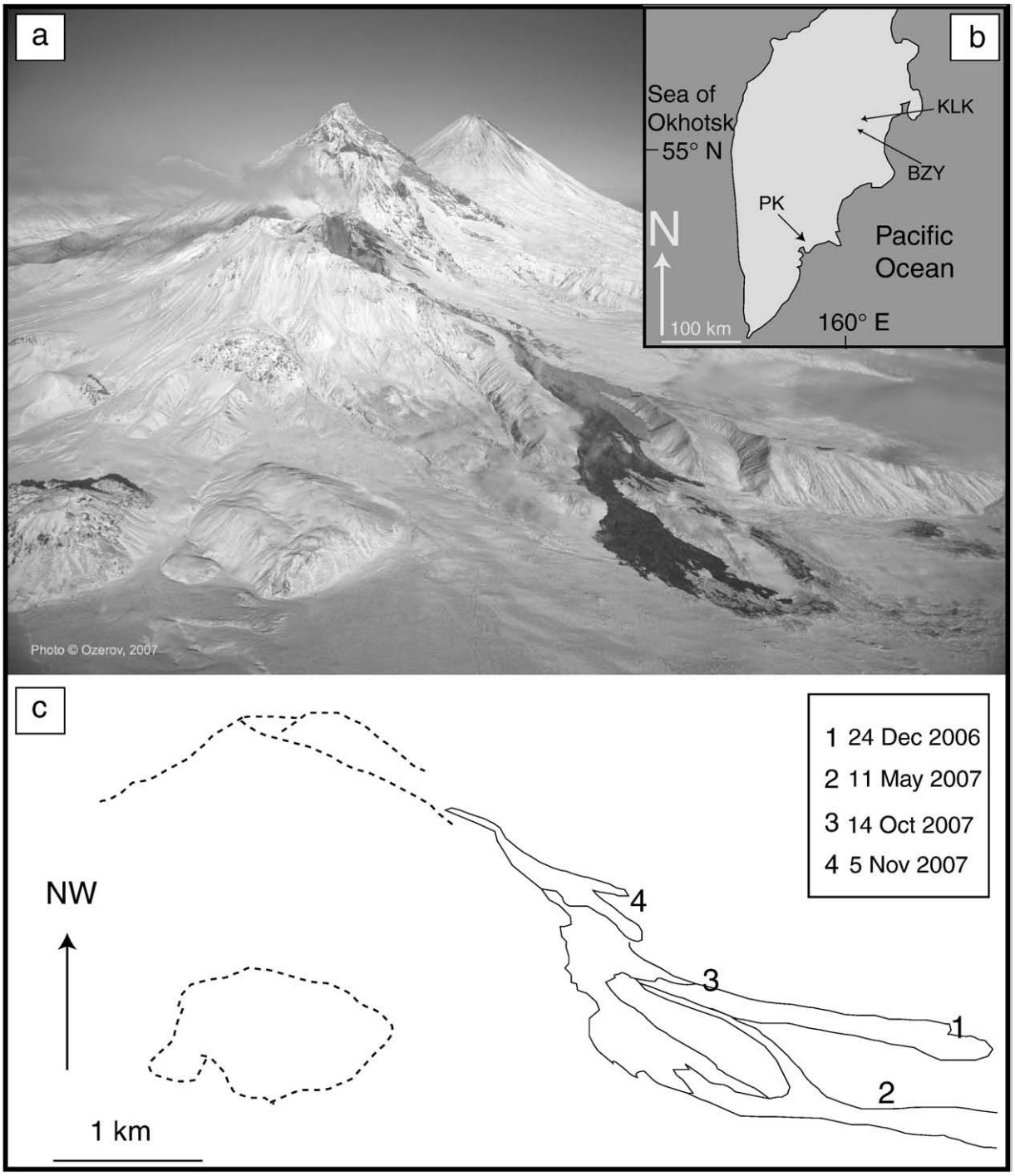

Fig. 1. (a) Helicopter-based photograph facing to the northwest. Pyroclastic flow deposits from the three eruptions (24 December 2006, 11 May 2007, and 14 October 2007) can be seen overlapping on the south-southeast flank. Following the October eruption, a dome-collapse deposit was emplaced on 5 November 2007. (b) Location map showing Bezymianny (BZY), Kluichevskoi (KLK), and the main city of Petropavlovsk–Kamchatsky (PK) are marked. (c) Traced outline of each PF deposit.

pyroclastic surge deposits (*e.g.* KVERT, 2007). Ashfall deposits are typically widely dispersed and are of low (*e.g.* centimetres) thickness (*e.g.* Francis, 1993). It is rapidly wind-blown, re-worked, and eroded, and is therefore rarely sampled directly. Similarly, pyroclastic surge deposits tend to have a low thickness, mantling topography. These too are commonly rapidly reworked and not easily sampled in primary form. Pyroclastic flow deposits typically have a higher erupted volume, are typically of greater thickness and follow pre-existing channels in topography (*e.g.* Francis, 1993). At Bezymianny, PF deposits are typically in the order of 4 to 8 km long, tens of metres in thickness, and remain largely in-tact on the time scale of several months to years (*e.g.* Belousov, 1996). Eruptions have never coincided with fieldwork (August 2004, August 2005, and August 2007), and therefore PF deposits serve as features that can be investigated in detail during field investigations.

1.2. The 24 December 2006 eruption

On December 24 2006 at 02:40 UTC, the Kamchatka Volcano Eruption Response Team (KVERT) raised the level of concern colour

code for Bezymianny Volcano from orange to red (KVERT, 2007). The colour codes are summarized in Table 1. According to KVERT, the red colour code indicates that a major explosive eruption is expected within 24 h or is already occurring, with associated strong earthquake activity (AVO, 2008). Such activity can also be associated with ash plumes reaching at least 7.5 km above sea level (a.s.l.). As predicted by this colour code change, Bezymianny Volcano erupted explosively at 09:17 UTC, 24 December 2006, generating a 10 km a.s.l. ash plume (Girina et al., 2006). The eruption also produced a PF deposit that extended 7.2 km to the southeast (Fig. 1c) and a short lava lobe, which was concentrated in a southwest-oriented depression on the lava dome (Carter et al., 2008).

1.3. The 11 May 2007 eruption

On 10 May 2007 the colour code for Bezymianny was raised from yellow to orange (KVERT, 2007). The orange alert implies that an explosive eruption is possible within a few days and may occur with little or no warning. In this case, ash plumes would not be expected to exceed 7.5 km a.s.l., although dome growth and the extrusion of lava are possible. On 12 May 2007, KVERT released a status report stating that, based on seismic data, an explosive eruption had occurred at Bezymianny on 11 May from 14:30 to 15:00 UTC (KVERT, 2007). Interpretation of seismic data from this event was complicated by noise from nearby Kluichevskoi volcano, which was also erupting at the same time. Multiple ash plumes were visible by residents over northern Kamchatka, which may have originated from either Bezymianny or Kluichevskoi. According to visual data (web camera) from Kozyrevsk village, 50 km west of the volcano, a hot avalanche occurred at Bezymianny on 11 May at 22:30 UTC, and on the same day an ash plume rose to 4 km a.s.l.. A thermal anomaly was observed in Moderate Resolution Imaging Spectroradiometer (MODIS) data, which has a TIR spatial resolution of 1 km. The anomaly extended several km to the southeast and was inferred to be caused by a hot PF deposit (KVERT, 2007) which is outlined in Fig. 1c.

1.4. The 14 October 2007 eruption and 5 November 2007 dome-collapse event

A high-intensity MODIS thermal anomaly was observed over Bezymianny's lava dome in the days preceding the 14 October 2007 eruption (KVERT, 2007). On 14 October 2007, KVERT raised the concern colour code from yellow to red. Based on the MODIS data, KVERT announced that a small eruption had occurred. According to seismic data, two eruptive events took place from 14:27–14:48 UTC and from 15:10–16:30 UTC on the same day. The PF deposit resulting from the eruptive events of 14 October 2007 is shown along with others in Fig. 1c. Ash plumes extended more than 100 km to the southeast and activity continued until approximately 14:00 UTC on 15 October. In the following days a new viscous lava flow was observed on the dome that was seen to be focussed in a channel leading south from the dome summit (Fig. 2a).

On 5 November 2007 from 08:43 till 10:10 UTC seismic data recorded a series of small explosions or collapse events from the front of a lava lobe. Two additional avalanches then occurred at 15:45 UTC and 18:07 UTC (KVERT, 2007). Field photographs by KVERT scientists confirmed on 21 October 2007 that a lava lobe was actively flowing in a channel south of the dome summit. The 5 November 2007 event was predominantly of "Merapi-type" collapse origin (*e.g.* Francis, 1993) due to the over-steepening and collapse of a lava flow front and therefore does not include it as an explosive eruption event during the 2006 to 2007 study period. The outline of the deposit created can be seen in Fig. 1c.

Table 1
KVERT level of concern colour codes, from the AVO website: http://www.avo.alaska.edu/color_codes.php.

Colour code	Description
Green	No eruption anticipated. Volcano is in quiet, "dormant" state.
Yellow	An eruption is possible in the next few weeks and may occur with little or no additional warning. Small earthquakes detected locally and (or) increased levels of volcanic gas emissions.
Orange	Explosive eruption is possible within a few days and may occur with little or no warning. Ash plume(s) not expected to reach 25,000 ft above sea level. Increased numbers of local earthquakes. Extrusion of a lava dome or lava flows (non-explosive eruption) may be occurring.
Red	Major explosive eruption expected within 24 h. Large ash plume(s) expected to reach at least 25,000 ft above sea level. Strong earthquake activity detected even at distant monitoring stations. Explosive eruption may be in progress.

2. Purpose

We build on our previous work at Bezymianny examining individual eruptions (Ramsey & Dehn, 2004; Carter, Ramsey, Belousov, 2007; Carter et al., 2008). Carter, Ramsey, Belousov (2007) examined the 11 January 2005 eruption, the emplacement of a summit lava lobe, and a short PF deposit that was emplaced. Following this, Carter et al. (2008) investigated the 24 December 2006 eruption and focussed research on satellite and ground-based studies of the PF deposit. Here, we analyzed new multi-temporal ASTER data from October 2006 to December 2007, which encompassed three discrete explosive eruptions and one collapse event at Bezymianny. The main purpose was to consider thermal and textural effects of actively cooling PF deposits at Bezymianny that have produced a complex overlapping series of deposits on the southeast flank. Ground-based thermocouple (*e.g.* Harris & Maciejewski, 2000) and Forward-Looking Infrared Radiometer (FLIR) thermal data (*e.g.* Patrick et al., 2007) were collected during a field campaign in August 2007 in order to detect changes in the May 2007 PF deposit. Together, the field measurements and ASTER data provide complementary validation for lower spatial resolution/higher temporal resolution Advanced Very High Resolution Radiometer (AVHRR) data (*e.g.* Dehn et al., 2000), which are used in the routine monitoring of North Pacific volcanoes by the Alaska Volcano Observatory (AVO).

3. Methods

3.1. ASTER data acquisition and image processing

ASTER is a spaceborne imaging sensor containing three spectral subsystems: visible/near infrared (VNIR), shortwave infrared (SWIR), and thermal infrared (TIR) (Yamaguchi et al., 1998). Each wavelength region can be used in combination to look at, for example, visual 2D and 3D changes in the VNIR (*e.g.* Stevens et al., 2004), high-temperature magmatic and fumarolic features in the SWIR (*e.g.* Pieri & Abrams, 2004), and lower-temperature fumarolic, magmatic degassing, and PF emplacement and cooling in the TIR (*e.g.* Ramsey & Dehn, 2004). ASTER has been used in several cases to interpret volcanic events at Bezymianny since its launch in 1999 (Ramsey and Dehn, 2004; Carter, Ramsey, Belousov, 2007; Carter, Ramsey, van Manen, 2007; Carter et al., 2008, 2009). The number of clear ground images in this area can be limited due to heavy snow cover in the winter and extensive cloud cover in the summer. Scheduling must also fit with the priorities of other scientific groups within the ASTER team. However, the pointing capability of ASTER allows for an increased number of images to be collected over target areas compared to other sensors (Abrams, 2000). In addition, at high latitudes (such as for Kamchatka), a greater number of images can be acquired due to overlapping orbit tracks.

From October 2006 to December 2007, 30 clear views of Bezymianny's dome and PF deposits were collected by ASTER and

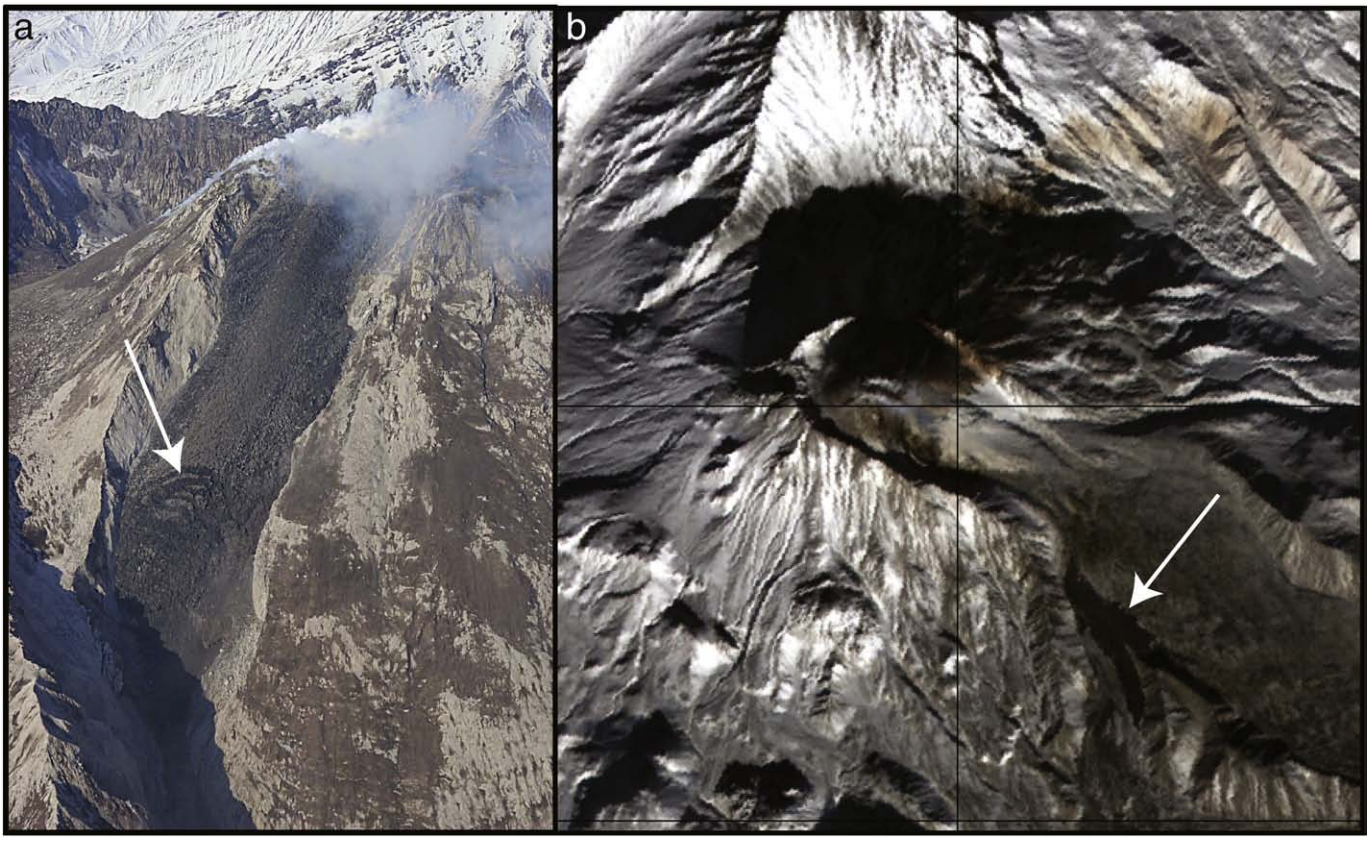

Fig. 2. (a) Oblique aerial photograph taken on 21 October 2007 facing northwest. An active lava flow was being emplaced at the time and travelled south within a pre-existing channel. Curved fractures were observed at the distal portion of the lava flow (see white arrow). Based on KVERT reports and ASTER image observations, the 5 November 2007 deposit was produced from the collapse of the lava flow front. Photograph courtesy of Yurii Demyanchuk. (b) ASTER daytime VNIR image from 13 November 2007 with a grid centred on 599,681 m E, 6,203,909 m N. A fresh PF deposit was detected on the southeast flank (see white arrow) that was low albedo and was, based on KVERT reports, considered to originate from the collapse of the lava flow front near the dome summit.

subsequently processed to level 2 (L2) surface kinetic temperature data. A standard MODTRAN atmospheric correction model was used with inputs from NCEP and estimates atmospheric scattering, emission, and downwelling radiance (Tonooka & Palluconi, 2005). The errors in accurate temperature retrieval from ASTER have been investigated (Gustafson et al., 2006) and were found to be accurate to within 2 °C.

The temperature and surface emissivity were extracted from the atmospherically corrected radiance product using the ASTER Temperature-Emissivity Separation (TES) algorithm (Gillespie et al., 1998). Within the TIR channels, ASTER has a noise equivalent delta temperature ($NE\Delta T$) of $\leq$0.3 K to accurately estimate surface temperatures and emissivity spectra (Gillespie et al., 1998). As the ASTER TIR $NE\Delta T$ value is so small, there would be no appreciable change in accuracy of extracted temperatures from cooler or hotter pixels, even pixels that are sub-zero (in °C). In addition, the 12-bit quantization of ASTER TIR data and relatively high dynamic range capable of recording temperatures up to 97 °C further assist in providing useful volcanological data (Abrams, 2000).

3.2. Field data

ASTER geometric performance has been assessed and found to be better than 0.1 pixels with respect to band-to-band registration and 0.2 pixels between each subsystem (Iwasaki & Fujisada, 2005; ASTER user's guide, 2007). Therefore, the maximum TIR systematic error would be ~9 m. Orthorectified daytime VNIR images are the highest spatial resolution and most geographically-accurate ASTER-derived data product. The orthorectification accuracy is 10–30 m in the *x*, *y*, *z* dimensions (Abrams, 2000). Therefore, one might expect a maximum positional error plus a band-to-band error of between 19 and 39 m for any daytime image, which is still within one ASTER TIR pixel. However, for nighttime data, the positional errors can be significantly larger (100's of metres). This is due to the processing software not having a corresponding higher resolution, solar-illuminated VNIR image.

Due to this inaccuracy in nighttime data, a simple solution to this problem was to geometrically relocate these nighttime images using a previously-collected orthorectified VNIR/TIR daytime image. A preliminary base map of the May 2007 deposit was created using an ASTER nighttime image from 30 June 2007. The orthorectified daytime VNIR and TIR images from 8 July 2007 were used to shift and correct the 30 June 2007 nighttime image 440 m east and 90 m north. Eight thermally-elevated pixels were selected from this image based on the criteria of being: (a) relatively high temperatures and (b) of approximately equal spacing along the PF deposit. The locations of each pixel were noted and used during the August field campaign.

The primary goal of the field work was to investigate thermal heterogeneities with distance from the summit along the May 2007 PF deposit. A secondary goal was to validate concurrent ASTER data (if there were minimal clouds) and to examine thermal anomalies detected in the previously-collected ASTER data. Seven of the eight selected pixels (herein numbered 1–7) were accessible and investigated in further detail. The corner coordinates of each 90 m ASTER pixel were located in the field, and FLIR images and/or thermocouple data were collected. Due to multiple field projects in the region, the FLIR camera was only available to survey pixels 4, 5, and 6. These were

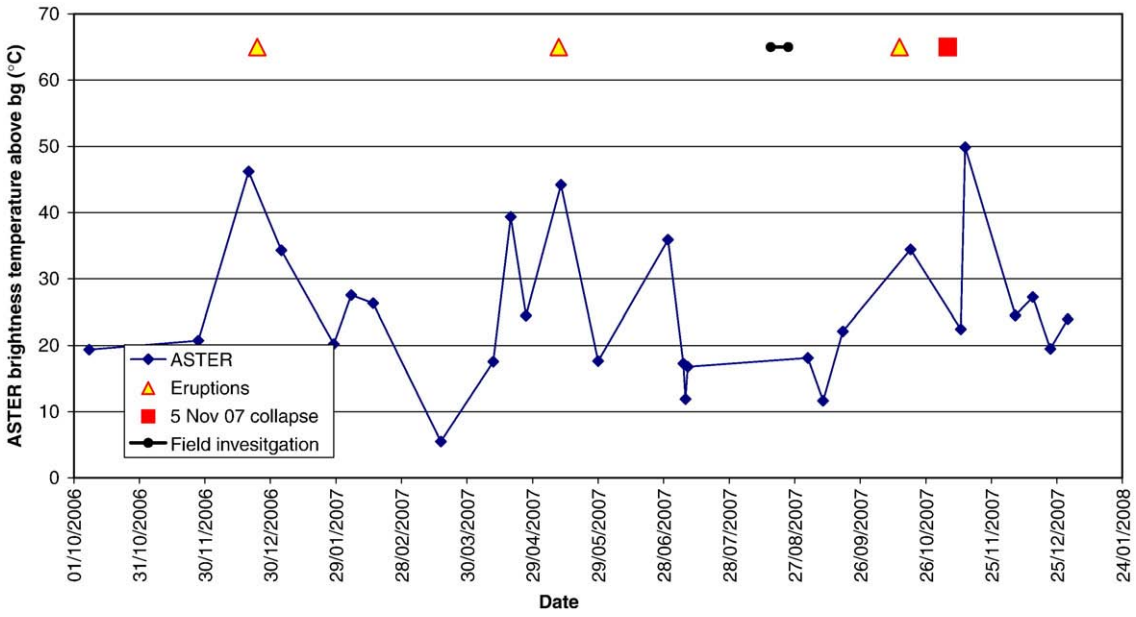

Fig. 3. ASTER TIR-derived maximum brightness temperature over the lava dome from October 2006 to December 2007. The actual eruption dates are denoted by the triangles. Significantly elevated brightness temperatures were noted around the times of the December 2006 and May 2007 eruptions. However, elevated temperatures were not detected prior to the October 2007 eruption, which may have been caused by clouds obscuring the dome. After Gustafson et al. (2006), ASTER temperatures were found to be accurate to within 2 °C, which provides an error margin on the data.

collected at a distance of 1 m from the surface facing vertically downwards for each corner and pixel centre. Individual temperature values and overall average temperatures were recorded. Direct surface kinetic temperatures were measured for all seven pixels using an Omega HH509 thermocouple. Temperatures of the PF deposit were also measured in each pixel corner and centre, with these measurements also being averaged. All pixels were assessed for surface covering by estimating the percentage of blocks, relative to ash on the surface. This was assessed using transects where measurements were made approximately every 3 m, running diagonally from corner to corner over each 90 m pixel. Radiant energy from non-isothermal pixels is averaged in a singular pixel-integrated value during an ASTER acquisition. Considering this fact as well as the lack of a synchronous ASTER image during the field campaign, care must be taken when comparing ASTER- and field-derived temperature data. However, the ASTER TIR images remained highly valuable prior to the field investigation to generate a base map that was used to define areas of interest to be examined in the field.

3.3. Aerial photography from November 2007

Aerial photography acquired in November 2007 (Fig. 1) helped to distinguish the four different PF deposits and facilitated our fieldwork investigation of the May 2007 PF deposit. Observations of the 24 December 2006 and 11 May 2007 eruptions are summarized in Carter et al. (2008) and Carter, Ramsey, Belousov (2007), respectively. However, there has been less work characterizing the October 2007 eruption. Aerial photographs from November 2007 (Fig. 1a) showed clear evidence of the PFs produced from each eruption and confirmed the presence of the newest PF. This deposit can be separated into two distinct units: (1) a low albedo unit that travelled a maximum of 6.4 km from the dome and then flowed in two directions around a topographic barrier in a similar manner to the May 2007 PF; and (2) a high albedo unit (or series of units) emplaced by a flow that travelled only 3.6 km from its source. It was noted by KVERT scientists that for the second and smaller event, the deposits appeared to contain predominantly dome-derived, non-juvenile material. The second deposit was therefore interpreted to be the product of the dome-collapse event on 5 November 2007.

4. Results

4.1. ASTER TIR-derived temperature data and analysis

Fourteen months of ASTER temperature data were collected from October 2006 to December 2007 over the summit lava dome (Fig. 3). Brightness temperature is a non-contact temperature measurement taken with an assumed emissivity of 1, and differs from kinetic temperature which is the true surface temperature of an object. Care must be taken when interpreting brightness temperature, which is affected by atmospheric conditions such as atmospheric temperature, humidity, and wind conditions. The maximum recorded TIR brightness temperature during the time period examined was ~50 °C above the background, well below the saturation temperature of ~97 °C (Yamaguchi et al., 1998). The average background temperature for each image was calculated from a non-thermally elevated background area of 50 × 50 TIR pixels (~20 km^2) at a similar elevation to the active dome. This value was used to derive the temperature above that background for the thermally-elevated regions. Three peaks in the temperature–time graph were noted around the time of the three eruptions (Fig. 3). Precursory signals were not detected for the October 2007 event, which may have been due to frequent cloud cover in the region at the time. Another reason may be due to limited pointing and tasking opportunities for the ASTER instrument at the time or the dome collapse event not being associated with any increase in thermal

Table 2
Pyroclastic flow results from each eruption using ASTER data.

PF date	24-Dec-06	11-May-07	14-Oct-07	5-Nov-07
PF perimeter distance (km)	13.24	13.71	10.63	4.79
PF area (km^2)	1.81	3.09	1.73	0.43
PF run out distance from dome summit (km)	7.20	7.00	6.40	4.78
ASTER image used	04-Jan-07	30-Jun-07	19-Oct-07	13-Nov-07
Number of days after eruption/event	11 days	50 days	5 days	8 days
Day/night	day	night	day	day
Averaged PF emissivity (ASTER bands 10–14)	0.936	0.972	0.944	0.955

output. Precursory thermal anomalies detected using ASTER may have been due to pre-explosive eruption lava spines, short lava flows, and/or vigorous degassing on the lava dome. However, more data such as field-based measurements (*e.g.* Belousov et al., 2002; Carter, Ramsey, Belousov, 2007) are typically necessary to interpret each event. Despite this, above-average thermal activity peaks were recorded during all three eruptive phases within the ASTER TIR data (Fig. 3). Eight days after the 5 November 2007 collapse, a maximum dome temperature above background of 49.9 °C was recorded. This may have been due to renewed activity at the dome after the collapse removed near-surface dome material, or that the collapse structurally altered the dome that later led to the effusion of a lava.

Statistics on the general properties of the three explosive eruption-derived PF deposits and the 5 November 2007 collapse deposit were collected and summarized in Table 2. The areas covered for the December 2006, May 2007, and October 2007 deposits were 1.8, 3.1 and 1.7 km^2, respectively, with run out distances of 7.2 km, 7 km, and 6.4 km. Area measurements of these deposits were calculated using the daytime VNIR images for the December 2006 and October 2007 deposits and from the TIR nighttime data for the May 2007 deposit because there was no corresponding VNIR image data for this deposit. Considering the difference in spatial resolution from the VNIR to TIR (15 m/pixel to 90 m/pixel), the accuracy of the May 2007 PF deposit area is therefore somewhat lower. Regardless, the May 2007 PF was over 1.5 times larger in surface area than the other deposits, based on ASTER observations.

Over the summit, an ASTER image from 19 October showed a distinct thermal anomaly over the southern part of the lava dome. This was caused by the emplacement of a lava lobe that later partially collapsed on 5 November 2007. Thus, ASTER observations detected another post-eruption lava lobe emplacement, in agreement with activity previously described by Belousov et al. (2002), Ramsey and Dehn (2004), Carter, Ramsey, Belousov (2007), and Carter et al. (2008). Following the 5 November 2007 collapse, an ASTER image from 13 November 2007 was collected and used to calculate the area of the deposit (0.43 km^2) and run out distance (4.78 km), confirming that this was the smallest of all the deposits studied (Fig. 2b). An excavated channel on the south part of the dome was also detected, indicating that this was the most likely origin point for the majority of the collapse deposit.

4.2. Field validation and textural characteristics of PF deposits and analysis of laboratory and ASTER emissivity data

Five band emissivity spectra were also extracted from the TIR radiance data for the three dates (Table 2) and the bulk emissivity value was calculated for each deposit. This information can be helpful inputs to thermal models of pyroclastic flow deposit cooling with time (*e.g.* Carter et al., 2008). For example, textural or vesicularity effects (*e.g.* Ramsey & Fink, 1999; Carter et al., 2009), or the density/thermal inertia information that relates to the proportion of blocks to ash within the PF can be better assessed. Carter et al. (2009) used block and ash samples from the March 2000 and January 2005 PF deposits. Laboratory TIR emission spectra were collected for samples and the emissivity profiles were compared to ASTER-derived spectra. In addition, field mapping with laboratory and satellite-derived spectra to infer the eruption style that created the two deposits. Thus, the analysis of derived emissivity spectra can be of great use in interpreting volcanological events.

An area of interest was selected over the spatial footprint of each PF deposit and associated spatial and spectral statistics were calculated for each band. These data were averaged producing a broadband emissivity value for each deposit (0.936, 0.972, 0.944, and 0.955 for December 2006, May 2007, October 2007, and November 2007, respectively). Twelve samples of blocks and ash were also collected from the May 2007 deposit and analyzed using the Fourier-Transform Infrared (FTIR) spectrometer at the University of Pittsburgh, following the methods of Ruff et al. (1997). In order to compare these laboratory data to ASTER broadband emissivity, the laboratory emissivity spectra for all the samples were convolved to the ASTER TIR bandpasses (8.3–11.3 μm). The laboratory-derived bulk emissivity was 0.953 compared to 0.972 for ASTER. The difference of 1.9% is well within the accuracy (3%) for ASTER-derived emissivity considering the errors in the instrument as well as errors arising from calibration and data correction for the atmosphere (Gillespie et al., 1998).

The overall composition within the PF deposits has remained relatively constant within the last ten years. Therefore, we do not believe that the compositional difference is the dominant factor explaining the emissivity variation seen. Furthermore, the 1.9% emissivity discrepancy is only slightly more than the inherent noise in the TIR, which is ~1.5% (Gillespie et al., 1998). Within a standard spectral library of emissivity data over geologic materials (*e.g.* the TES laboratory, Arizona State University or the spectral library included with the ENVI image processing software), the total variation in emissivity values is around 30% (*e.g.* Christensen et al., 2000). The inherent noise in both data collection methods and slight errors in atmospheric correction (of the ASTER data) probably accounts for the small discrepancy observed.

The broadband emissivity data is therefore useful for thermal models of PF deposits cooling with time (*e.g.* Carter et al., 2009); for better understanding of varying textural, vesicularity, and cavity effects (*e.g.* Ramsey & Fink, 1999); as well as density-dependent thermal inertia effects on the deposit as it relates to the proportion of blocks and ash within the PF.

4.3. Analysis of the May 2007 pyroclastic flow deposit

Typically, each Bezymianny PF deposit consists of juvenile or older, hydrothermally altered blocks set in a matrix of compacted ash (Carter et al., 2009). This investigation was intended to further investigate the thermal and textural characteristics of recent PF deposits, focussing on the May 2007 deposit. An ASTER thermal infrared nighttime image from 30 June 2007 was used to spatially locate and register the May

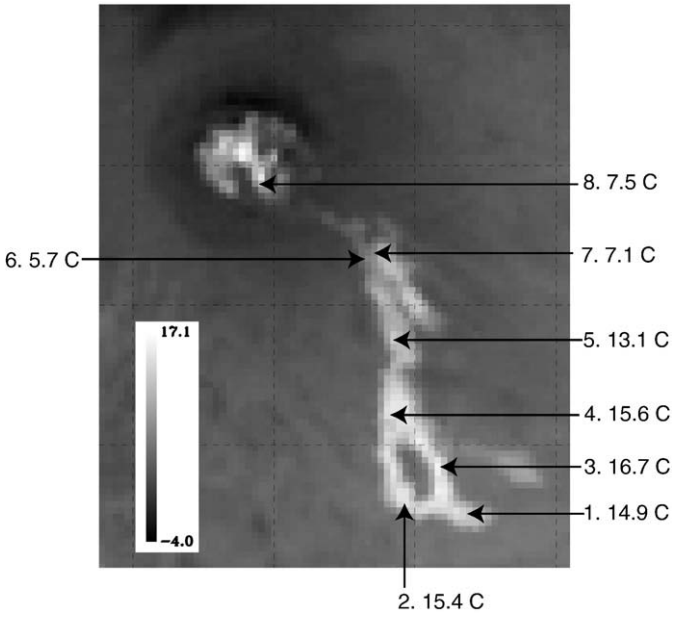

Fig. 4. ASTER 30 June 2007 nighttime brightness temperature (Celsius) image showing with the thermally-elevated dome region as well as the area covered by the May 2007 PF deposit. Also shown are the eight pixels that were chosen for further field investigation, the first seven of which were visited in the field in August 2007. 2 km grid overlain with north upwards.

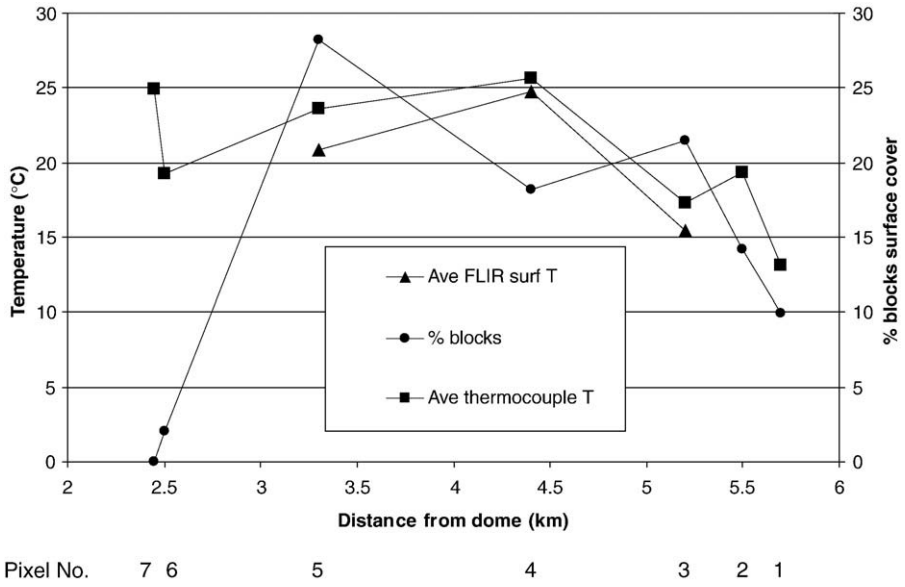

Fig. 5. Field data of the May 2007 PF deposit collected on the seven pixels denoted in Fig. 4. The averaged FLIR brightness temperatures and thermocouple kinetic temperatures data for pixels 1 to 5 show a positive correlation. The percentage of blocks (second *y*-axis) also shows a general correlation with temperature indicating the strong effect of thermal inertia. In the pixels closer to the dome (numbers 6 and 7) the slope is much steeper and no large accumulation of blocks was possible. ASTER data were not available during the field campaign due to heavy cloud cover.

2007 PF deposit pixels (1–7) in the field (Fig. 4). The last pixel was on the dome itself and was inaccessible due to ongoing activity. FLIR and thermocouple temperature data were collected for pixels 3, 4, and 5, in addition to the percentage of all blocks for each location except for pixel 8 (Fig. 5).

At a distance of 2.5 km from the dome (training pixels 7 and 6), elevated thermocouple-derived temperatures were recorded over highly ash-rich surfaces containing less than 5% blocks. Slope angles were higher in this area, gradually lessening with distance from the dome. For the three intermediate-distance training pixels (5, 4, and 3), FLIR, thermocouple, and surface block cover were collected. FLIR and thermocouple data were within 3 °C of each other and a high proportion of blocks (>15% ground cover) was observed. The maximum temperatures from FLIR and thermocouple data were recorded over training pixel 4 at around 4.3 km from the dome. For the distal training pixels (3, 2, and 1), a distinct temperature drop was recorded beginning around 5 km from the dome. This drop also coincided with areas containing a lower proportion of surface blocks.

We interpret that close to the summit, the surface was dominated by ash fallout from the PF on higher slope angles where blocks were not as able to easily accumulate. Higher thermocouple temperatures recorded for these areas may reflect an increased thickness, or may have been affected by remnant heat from the December 2006 PF deposit directly below. The main body of the PF contained the highest temperatures and a higher percentage of blocks. As the PF bifurcated around a topographic high point on the slope, a loss of momentum may have promoted the deposition of blocks, which retained more heat. Toward the PF distal margin, all temperatures dropped significantly (>10 °C) over a relatively short distance (<1 km). The thermocouple-derived temperature range within training pixel 2 was 34 °C, the greatest range within all training pixels. The training pixel 2 centre surface temperature was acquired over a vapour-phase, rootless fumarole area of the PF deposit, which increased the average pixel value over the five measurements (four corners and centre). Without this one measurement, the average would have only been 14 °C. Thus, the trend in the thermocouple data from pixel 3 to pixel 1 was a gradual negative slope towards the PF terminus.

At the PF terminus, steam explosion/degassing craters were likely formed after the PF was emplaced (Carter, Ramsey, Belousov, 2007; Fig. 6a). Temperatures as high as 225 °C were recorded inside the

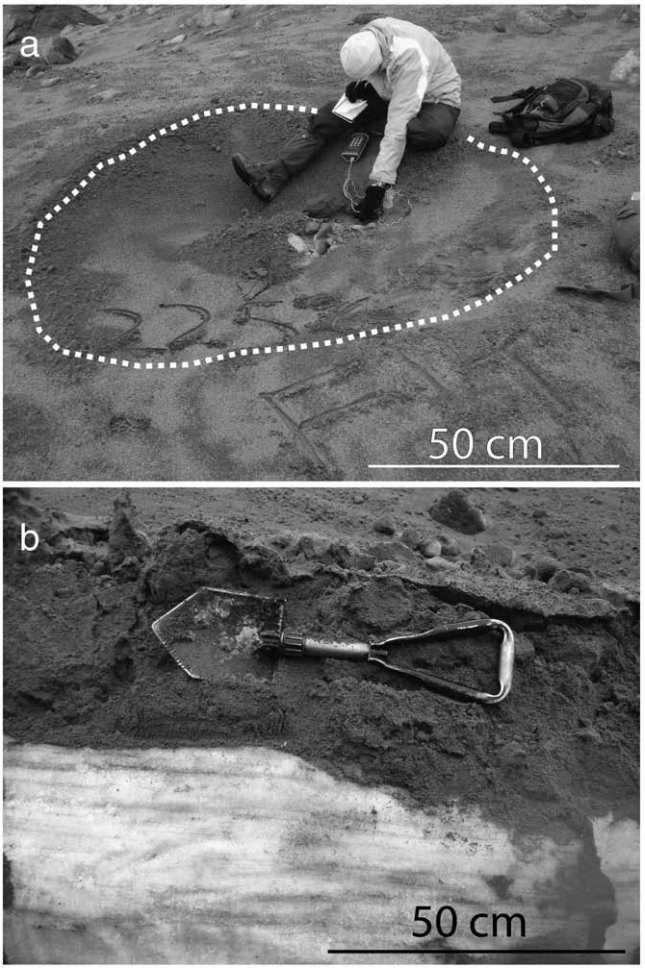

Fig. 6. Field photographs near the May 2007 PF terminus. (a) Southwest-facing photograph of a steam explosion crater, over 1 m in diameter. The maximum temperature recorded was 225 °C. (b) Snow layer underneath the PF deposit, with flow direction to the right (southeast).

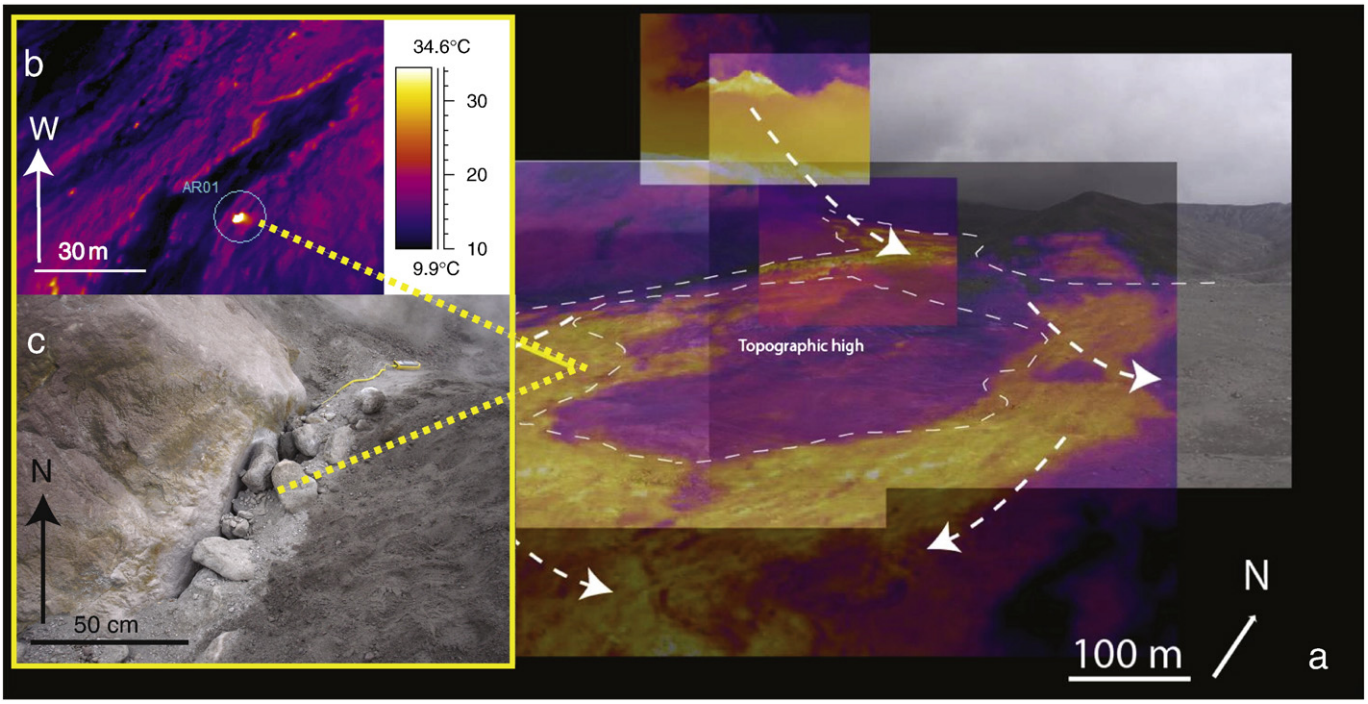

Fig. 7. Field-based thermal observations. (a) Oblique aerial photograph composite taken from the southeast flank facing northwest towards the dome. FLIR images of the dome region and May 2007 PF deposit are overlain to show the relationship of the topographic high with the emplacement of the PF. (b) Aerial, near-vertical FLIR image showing the same fumarole. (c) Field photograph of fumarole 5 km from the summit with the maximum temperature (377 °C recorded with a thermocouple).

vapour-phase, rootless fumarole centres. The PF terminus was relatively abrupt (over 5–10 m) and was emplaced on to a fluvially-deposited outwash plain. On the southern border of the PF (between training pixels 1 and 2), a snow layer was observed directly beneath the PF deposit that contained incised tunnels created by melt water (Fig. 6b). We interpret that the terminus underwent more rapid

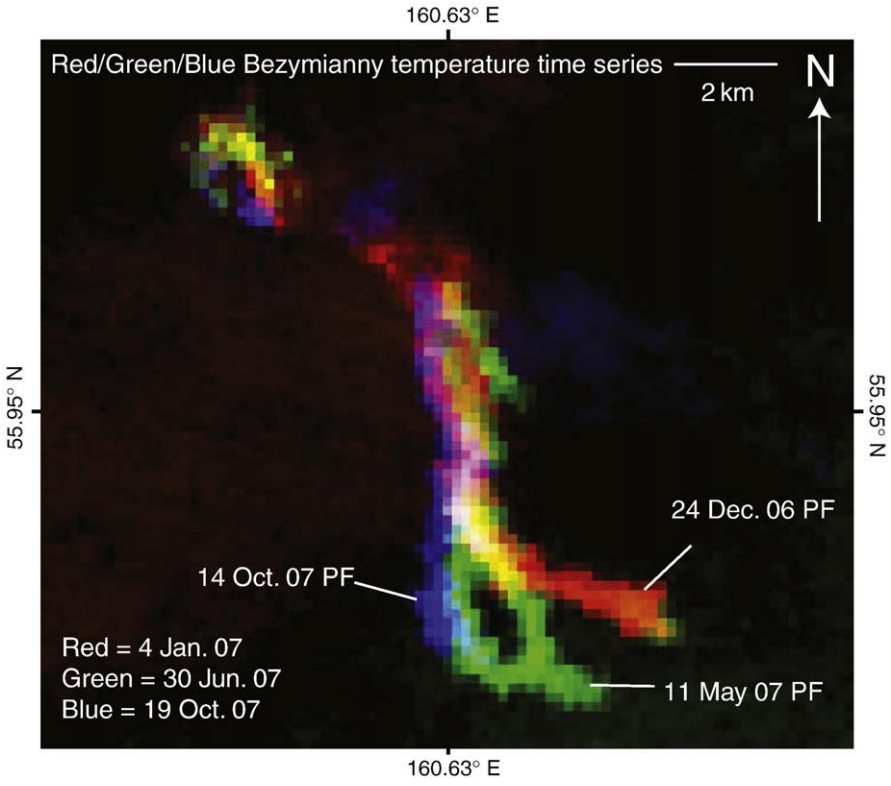

Fig. 8. Three colour (red, green, and blue) temporal composite of ASTER TIR temperature data from 4 January (red), 30 June (green), and 19 October (blue). The dome region (upper left) was thermally-elevated in the northwest region of the dome on 4 January and 30 June 2007 (yellow), but by 19 October, this region had shifted to the southern portion of the dome. Three pyroclastic flows were accurately geolocated with respect to each date. The deposits from the eruptions of 24 December 2006, 11 May 2007, and 14 October 2007, can be clearly seen.

cooling (relative to training pixels 4 to 7) due to: (a) the proportion of blocks (and hence the bulk density) of the PF was lower (Fig. 5); (b) the lower portion of the PF (between training pixels 2 and 1) was emplaced on to snow (Fig. 6). Over a time period of weeks to months, the cooler substrate, and subsequent melting likely promoted heat loss on the PF.

Several vapour-phase fumaroles were observed that were warmer than the majority of the surface of the PF deposit. The warmest fumarole was measured at 377 °C and was located on the southeast branch of the PF deposit. It was within 5 m from the edge of the PF lobes and 5 km from the dome summit (Fig. 7). This fumarole was also observed in the aerial FLIR data as a clear thermal anomaly (Fig. 7b). Such high temperatures three months after its eruption and emplacement suggest that the deposit must have been of sufficient thickness and/or bulk density to retain large amounts of heat. Considering the fact that the May 2007 PF covered a larger surface area than the other deposits, this high temperature implies that the deposit was also of greater thickness and larger total volume.

A composite of three ASTER TIR images (acquired on 4 January, 30 June, and 19 October 2007) shows the overlapping PF deposits (Fig. 8). This image composite is useful for visually analyzing the accumulation of these three PF deposits over the 2006–7 time period. Also, this dataset adds to the digital archive of ASTER thermal anomalies caused by eruptions at Bezymianny during the 2000 to 2008 time period. This further highlights the importance of such multispectral, moderate spatial resolution orbital data for volcanic monitoring.

5. Summary and concluding remarks

Fourteen months of ASTER data were used to produce a moderate spatial, spectral, and temporal resolution dataset characterizing eruptive activity at Bezymianny. The dimensions and characteristics of each PF were analysed accordingly. The May 2007 PF was over 3 km^2 and was 1.5 times larger than the December 2006 and October 2007 PF deposits. The ASTER-derived emissivity results differed by only 1.9% from the laboratory-derived data and were within the noise level of ASTER. This provided a validation of the ASTER surface emissivity data product and a range of broadband emissivity values for compositionally similar (andesitic), but texturally varying, young PF deposits. Based on the field-derived temperature data and surface block percentages (Fig. 5), we interpret that the May 2007 PF deposit was more block-rich in the medial portion of the flow surface, but more ash-dominated at the PF terminus region, which promoted more rapid cooling. Compared to the December 2006 deposit that had a block-rich terminus (Carter et al., 2008), the May 2007 PF deposit had a more gradational, ash-dominated terminus. This may have been caused by a topographic barrier that separated and diverted the PF and forced the emplacement of blocks around this barrier (*i.e.* near training pixels 3 and 4).

At the PF terminus, several explosion/degassing craters were found on the surface in the same area as a snow layer beneath the PF. We interpret that phreatic explosions generated the craters as the PF encountered the snow layer. In addition, the snow layer would have promoted more rapid heat loss after emplacement, which may explain the lower-temperature range between the ASTER, FLIR, and thermocouple datasets.

The synthesis of ASTER and field data suggests the deposit contained: (1) a block-rich thicker central region approximately 5 km from the vent, (2) an area upslope and around the topographic high point that contained the most blocks and that was the greatest thickness, and (3) the PF terminus contained explosion craters, a low block percentage, and was emplaced on to snow.

Three explosive eruptions and an additional dome-collapse event were detected and ASTER multi-temporal TIR image composite was used to provide a geospatial footprint for each of these PF deposits. This remote sensing data analysis, combined with the field data have proven highly valuable for interpreting repeated volcanic eruptions and PF deposits at Bezymianny. More specifically, ASTER data provides valuable quantitative volcanological data on the time scale of days to weeks that can be used to analyze variations in activity. There is a continued need to monitor volcanoes in the North Pacific, many of which are difficult or impossible to access and have very limited or no ground-based observations. The analytical methods and data analysis results presented in this study can be carried out in conjunction with local Russian (KVERT) and Alaskan (AVO) groups to facilitate information transfer between agencies, government bodies, and the aviation industry.

Acknowledgements

This work was funded partially by grants to M.S.R. from the National Aeronautics and Space Administration (NASA) (grant NNG04GO69G), the ASTER Science Team, and the National Science Foundation (NSF) (grant EAR-0309631). AJC acknowledges the support of the Andrew Mellon Fellowship, the Henry Leighton Memorial Scholarship. The authors also acknowledge the financial assistance provided by National Geographic for field logistics and travel. The authors thank Alexei Ozerov for the photograph used in Fig. 1 and for continued logistical support in the field. The authors also thank Valerio Lombardo and an anonymous reviewer for helpful and detailed comments that greatly improved the manuscript. AJC thanks Andrea Steffke for fruitful discussions and advice. Thanks also to Olga Girina, Yuri Demyanchuk, Evgenni Gordeev, and Oxana Evdokimova at the Institute of Volcanology and Seismology, (IVS), Russia, and Jill Shipman at the University of Alaska, Fairbanks (UAF).

References

Abrams, M. (2000). The Advanced Spaceborne Thermal Emission and Reflectance Radiometer (ASTER): Data products for the high spatial resolution imager on NASA's Terra platform. *International Journal of Remote Sensing*, *21*, 847−859.

ASTER user's guide, part II (2007). Earth Remote Sensing Data Analysis Center (ERSDAC). http://www.science.aster.ersdac.or.jp/en/documnts/users_guide/part1/pdf/Part2_5.1E.pdf

Alidibirov, M. A., Bogoyavlenskaya, G. E., Kirsanov, I. T., Firstov, P. P., Girina, O. A., Belousov, A. B., Zhdanova, E. Yu., & Malyshev, A. I. (1990). The 1985 eruption of Bezymianny. *Volcanology and Seismology*, *10*, 839−863.

Alaska Volcano Observatory (AVO) colour code website (2008). (http://www.avo.alaska.edu/color_codes.php).

Belousov, A. B. (1996). Deposits of the 30 March 1956 directed blast at Bezymianny Volcano, Kamchatka, *Russia*. *Bulletin of Volcanology*, *57*, 649−662.

Belousov, A., Voight, B., & Belousova, M. (2007). Directed blasts and blast-generated pyroclastic density currents: A comparison of the Bezymianny 1956, Mount St Helens 1980, and Soufrière Hills, Montserrat 1997 eruptions and deposits. *Bulletin of Volcanology*, *69*, 701−740.

Belousov, A., Voight, B., Belousova, M., & Petukhin, A. (2002). Pyroclastic surges and flows from the 8–10 May 1997 explosive eruption of Bezymianny Volcano, Kamchatka, Russia. *Bulletin of Volcanology*, *64*, 455−471.

Bogoyavlenskaya, G. E., Braitseva, O. A., Melekestsev, I. V., Maksimov, A. P., & Ivanov, B. V. (1991). Bezymianny Volcano. In S. A. Fedotov & Y. U. P. Masurenkov (Eds.), *Active volcanoes of Kamchatka*, *vol. 1*. (pp. 195−197)Moscow: Nauka.

Bogoyavlenskaya, G. E., & Kirsanov, I. T. (1981). Twenty five years of volcanic activity of Bezymianny.*Volcanology and Seismology*, *2*, 3−13 (in Russian).

Carter, A. J., Girina, O. A., Ramsey, M. S., & Demyanchuk, Yu. V. (2008). ASTER and field observations of the 24 December 2006 eruption of Bezymianny Volcano, Russia. *Remote Sensing of Environment*, *112*, 2569−2577.

Carter, A. J., Ramsey, M. S., & Belousov, A. B. (2007). Detection of a new summit crater on Bezymianny Volcano lava dome: Satellite and field-based thermal data. *Bulletin of Volcanology*, *69*, 811−815.

Carter, A. J., Ramsey, M. S., Durant, A. J., Skilling, I. P., & Wolfe, A. L. (2009). Micron-scale roughness of volcanic surfaces from thermal infrared spectroscopy and scanning electron microscopy. *Journal of Geophysical Research*, *114*, B02213. doi:10.1029/2008JB005632

Carter, A. J., Ramsey, M. S., & van Manen, S. M. (2007). Thermal infrared investigation of the pyroclastic flow deposits and dome region of Bezymianny Volcano, Kamchatka, Russia. *Eos Trans. American Geophysical Fall Meeting (abs. V21A-0386)*.

Christensen, P. R., Bandfield, J. L., Hamilton, V. E., Howard, D. A., Lane, M. D., Piatek, J. L., Ruff, S. W., & Stefanov, W. L. (2000). A thermal emission spectral library of rock-forming minerals. *Journal of Geophysical Research*, *105*, 9735−9739.

Dehn, J., Dean, K., & Engle, K. (2000). Thermal monitoring of North Pacific volcanoes from space. *Geology*, *28*, 755−758.

Francis, P. (1993). *Volcanoes: A planetary perspective*. New York: Oxford University Press.

Gillespie, A., Rokugawa, S., Matsunaga, T., Cotherm, J. S., Hook, S., & Kahle, A. B. (1998). A temperature and emissivity separation algorithm for Advanced Spaceborne

Thermal Emission and Reflection Radiometer (ASTER) images. *IEEE Transactions on Geoscience and Remote Sensing*, *36*, 1113—1126.

Girina, O. A., Senyukov, S. L., Malik, N. A., Manevich, A. G., Ushakov, S. V., Mel'nikov, D. V., et al. (2006). Activity of Kamchatkan and Northern Kuriles (Paramushir Island) volcanoes, Vestnik KRAUNC. *Sciences of the Earth*, *2*. (pp. 151—157) http://www.kscnet.ru/kraesc/2006/2006_8/art13.pdf

Gorshkov, G. S. (1959). Gigantic eruption of the Bezymianny Volcano. *Bulletin of Volcanology*, *20*, 77—109.

Gustafson, W. T., Gillespie, A. R., & Yamada, G. (2006). Revisions to the ASTER temperature/emissivity separation algorithm. In J. A. Sobrino (Ed.), *Second Recent Advances in Quantitative Remote Sensing* (pp. 770—775). Spain: Publicacions de la Universitat de València ISBN: 84-370-6533-X; 978-84-370-6533-5.

Harris, A. J. L., & Maciejewski, A. J. H. (2000). Thermal survey's of the Vulcano Fossa fumarole field 1994–1999: Evidence for fumarole migration and sealing. *Journal of Volcanology and Geothermal Research*, *102*, 119—147.

Iwasaki, A., & Fujisada, H. (2005). ASTER geometric performance. *IEEE Transactions on Geoscience and Remote Sensing*, *43*, 2700—2706.

Kamchatka Volcanic Eruption Response Team (KVERT) Report (2007). Bezymianny Volcano. 10 May 2007 UTC (http://www.avo.alaska.edu/activity/avoreport.php).

Miller, T. P., & Casadevall, T. J. (2000). Volcanic ash hazards to aviation. In H Sigurdsson, BF Houghton, S McNutt, H Rymer, & J Stix (Eds.), *Encyclopedia of volcanoes* (pp. 915—930). San Diego, CA: Academic Press.

Papp, K. P., Dean, K. G., & Dehn, J. (2005). Predicting regions susceptible to high concentrations of airborne volcanic ash in the North Pacific region. *Journal of Volcanology and Geothermal Research*, *148*, 295—314.

Patrick, M. R., Harris, A. J. L., Ripepe, M., Dehn, J., Rothery, D., & Calvari, S. (2007). Strombolian explosive styles and source conditions: Insights from thermal (FLIR) video. *Bulletin of Volcanology*, *69*, 769—784.

Pieri, D., & Abrams, M. (2004). ASTER watches the world's volcanoes: A new paradigm for volcanological observations from orbit. *Journal of Volcanology and Geothermal Research*, *135*, 13—28.

Ramsey, M. S., & Dehn, J. (2004). Spaceborne observations of the 2000 Bezymianny, Kamchatka eruption: The integration of high-resolution ASTER data into near real-time monitoring using AVHRR. *Journal of Volcanology and Geothermal Research*, *135*, 127—146.

Ramsey, M. S., & Fink, J. H. (1999). Estimating silicic lava vesicularity with thermal remote sensing: A new technique for volcanic mapping and monitoring. *Bulletin of Volcanology*, *61*, 32—39.

Ruff, S. W., Christensen, P. R., Barbera, P. W., & Anderson, D. L. (1997). Quantitative thermal emission spectroscopy of minerals: A laboratory technique for measurement and calibration. *Journal of Geophysical Research*, 14,899—14,913.

Stevens, N. F., Garbeil, H., & Mouginis-Mark, P. J. (2004). NASA EOS Terra ASTER: Volcanic topographic mapping and capability. *Remote Sensing of Environment*, *90*, 405—414.

Tonooka, H., & Palluconi, F. D. (2005). Validation of ASTER/TIR standard atmospheric correction using water surfaces. *IEEE Transactions on Geoscience and Remote Sensing*, *43*, 2769—2777.

Yamaguchi, Y., Kahle, A. B., Tsu, H., Kawakami, T., & Pniel, M. (1998). Overview of Advanced Spaceborne Thermal Emission and Reflection Radiometer (ASTER). *IEEE Transactions on Geoscience and Remote Sensing*, *36*, 1062—1071.